Electronic Supplementary Material (ESI) for Polymer Chemistry.
This journal is © The Royal Society of Chemistry 2021

Supporting Information

Interlayer hydrogen bond-assisted poly(perylene diimides) photocatalysts to improve the oxygen evolution under visible light

Shufan Feng[a], Zhiqiang Wang[b], Huihui Xu[a], Sifan Li[a], Xueqing Gong [b] and Jianli Hua[*a]

[a] *Key Laboratory for Advanced Materials, Joint International Research Laboratory for Precision Chemistry and Molecular Engineering, Feringa Nobel Prize Scientist Joint Research Center, School of Chemistry and Molecular Engineering, East China University of Science & Technology, 130 Meilong Road, 200237, Shanghai, China.*

[b] *Key Laboratory for Advanced Materials and Joint International Research Laboratory for Precision Chemistry and Molecular Engineering, Centre for Computational Chemistry and Research Institute of Industrial Catalysis, School of Chemistry and Molecular Engineering, East China University of Science and Technology, 130 Meilong Road, Shanghai 200237, PR China.*

* Corresponding author. Tel.: +86 21 64250940; fax.: +86 21 64252758.

E-mail address: jlhua@ecust.edu.cn (J. Hua)

Table of Contents

1. Structural characterization of poly(PDI)s

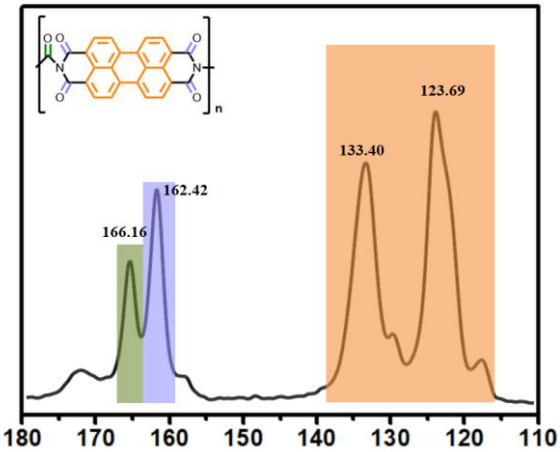

Fig. S1 Solid state ^{13}C NMR spectrum of **U-PDI**.

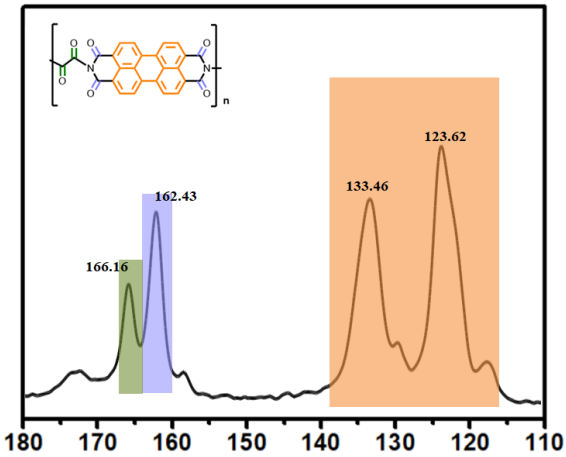

Fig. S2 Solid state ^{13}C NMR spectrum of **OA-PDI**.

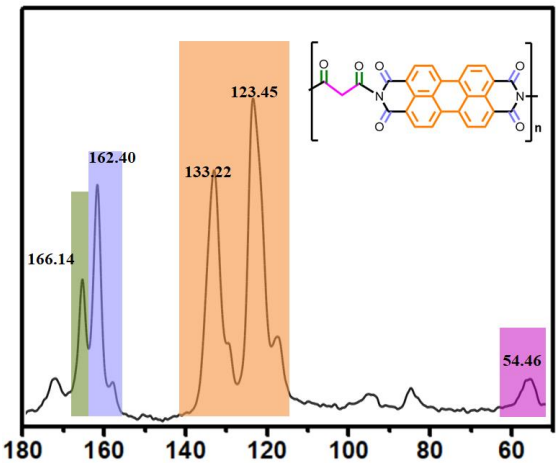

Fig. S3 Solid state ^{13}C NMR spectrum of **MA-PDI**.

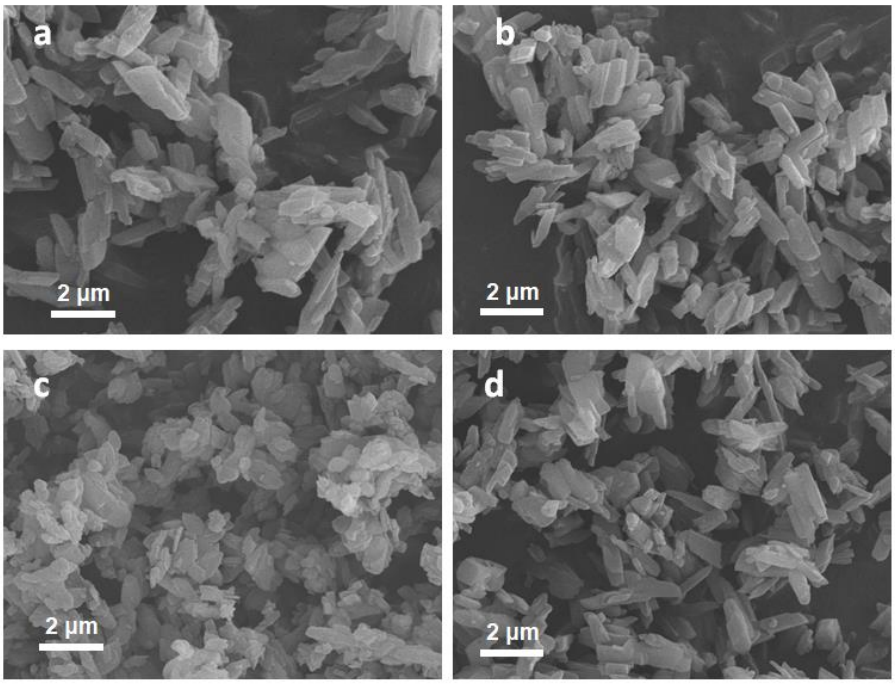

Fig. S4 SEM image of the **U-PDI** (a), **OA-PDI** (b), **MA-PDI** (c) and **BU-PDI** (d).

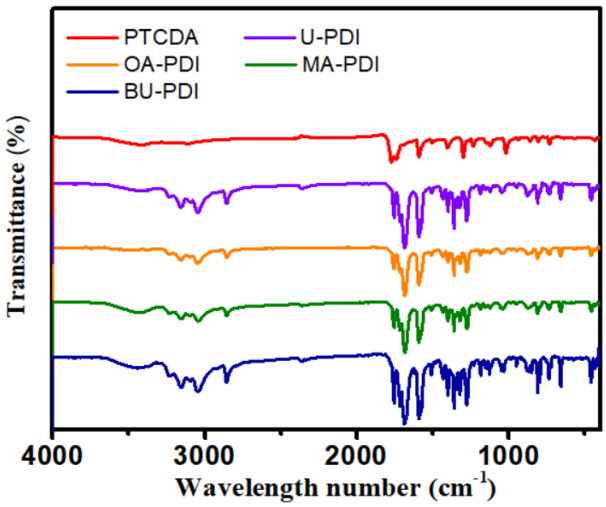

Fig. S5 Full range IR spectra of poly(perylene diimides).

Table S1. Full width at half maximum (FWHM) of **U-PDI**, **OA-PDI**, **MA-PDI** and **BU-PDI**

Sample	U-PDI	OA-PDI	MA-PDI	BU-DPI
FWHM	0.49	0.48	0.60	0.45

2. The oxygen origin determination by ^{18}O isotope

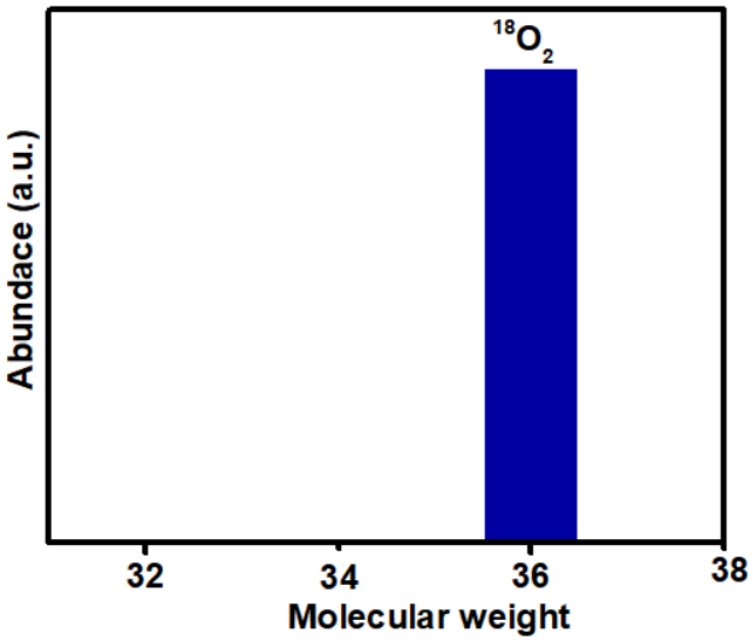

Fig. S6 The oxygen origin determination by ^{18}O isotope.

3. Effect of metal oxide cocatalyst on oxygen production

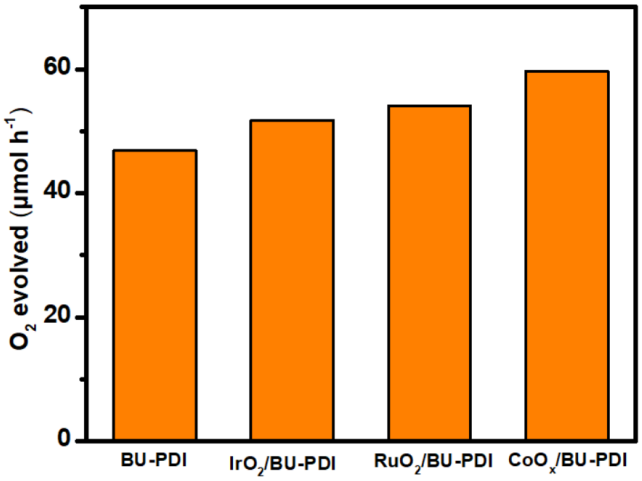

Fig. S7 The comparison of photocatalytic O_2 evolution rate over **BU-PDI** with different co-catalysts.

4. Stability test for Photocatalytic oxygen production

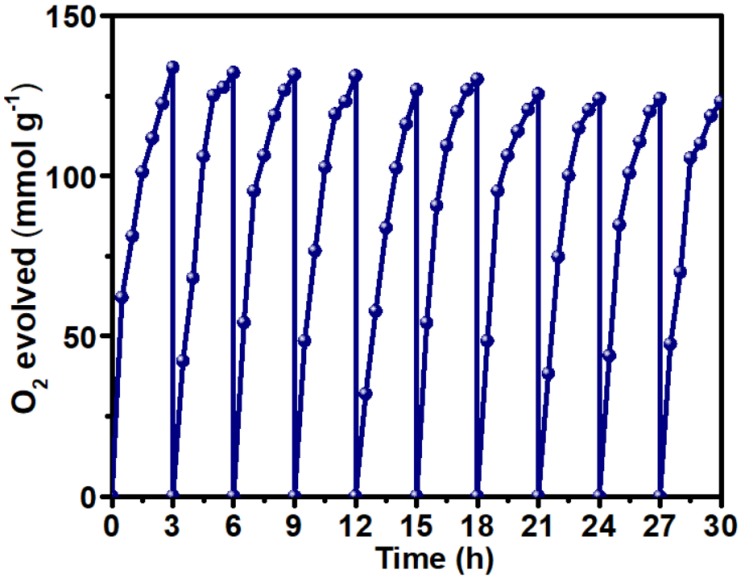

Fig. S8 Cycling runs in the photocatalytic oxygen evolution of **BU-PDI.**

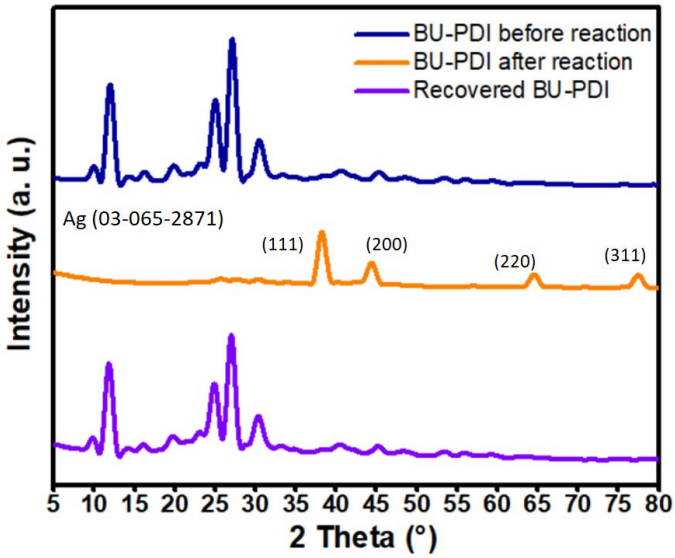

Fig. S9 XRD spectrum of **BU-PDI** before and after photocatalysis experiment.

5. Charge transfer kinetics research

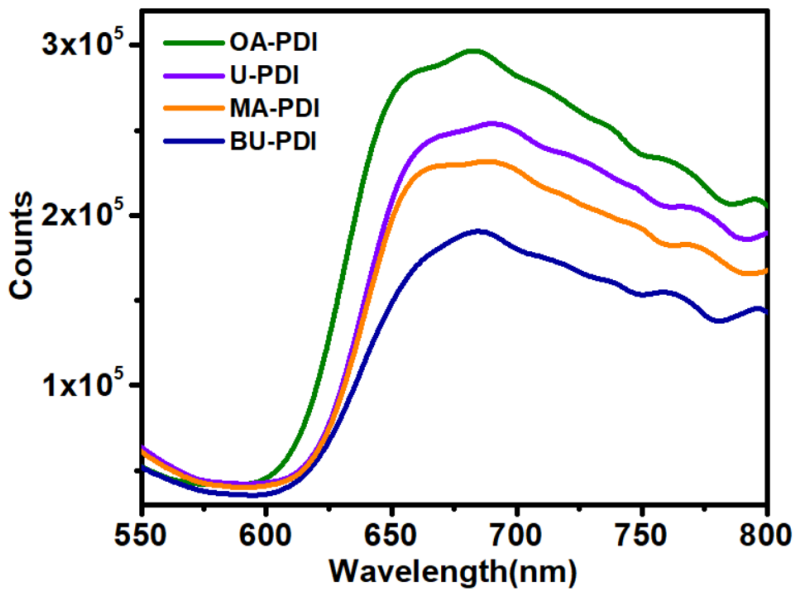

Fig. S10 PL spectra of **U-PDI**, **OA-PDI** , **MA-PDI** and **BU-PDI**.

Table S2. Simulation of electrochemical impedance spectra (EIS).

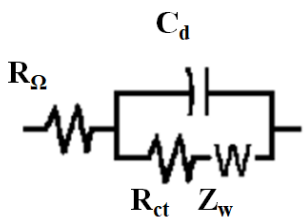

Sample	MA-PDI	U-PDI	OA-PDI	BU-PDI
R_Ω/Ω	9.71	9.97	15.89	15.06
C_d/F	1.18×10^{-5}	8.45×10^{-6}	5.30×10^{-6}	7.69×10^{-6}
$R_{ct}/k\Omega$	8.09	7.65	6.30	3.29
Z_w/Ω	9.00×10^{-5}	8.19×10^{-5}	9.60×10^{-5}	9.00×10^{-5}

6. Surface charge density and Open circuit potential measurement

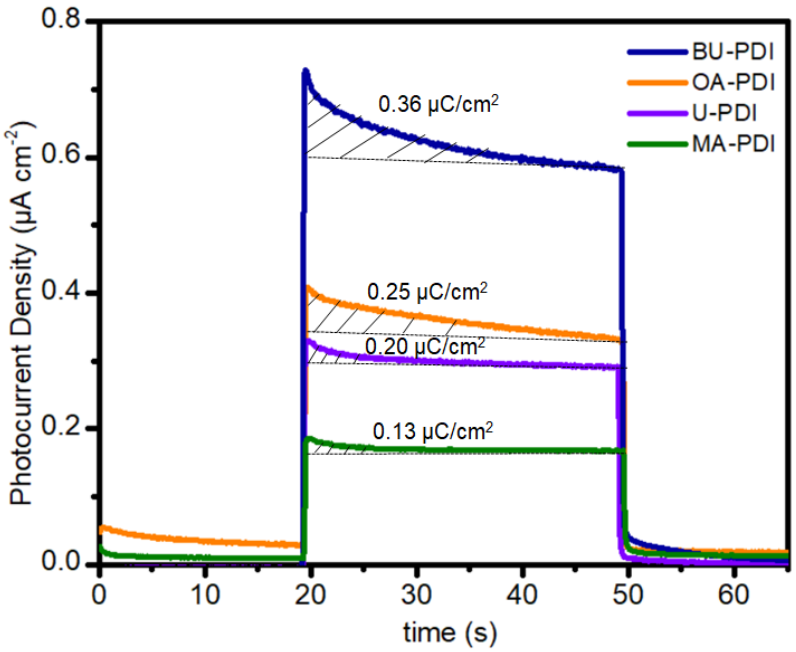

Fig. S11 The surface charge density of **U-PDI**, **OA-PDI**, **MA-PDI** and **BU-PDI.**

Table S3. Open circuit potential of **U-PDI**, **OA-PDI** , **MA-PDI** and **BU-PDI**

Sample	U-PDI	OA-PDI	MA-PDI	BU-DPI
Open circuit potential (vs. NHE)	0.468	0.434	0.425	0.508

7. Structure characterization and performance of EA-PDI

The synthesis of **EA-PDI** is according to literature reported before.[1] The structure of **EA-PDI** is characterized by FT-IR and solid-state ^{13}C NMR spectroscopy. In ^{13}C NMR spectroscopy, the peaks for carbonyl group (161.92 ppm) and conjugated carbon (133.83 and 121.77 ppm) on the PDI ring can be observed. Besides, the peak of the ethyl group can be observed at 55.23 ppm of the high field, which indicated the formation of ethylenediamine-PDI polymers. Besides, unpolymerized PTCDA shows two broad IR vibrational bands at 1739 cm^{-1} and 1768 cm^{-1} for ν(C=O) of anhydride, whereas **EA-PDI** exhibited two distinct peaks at around 1665 cm^{-1} and 1691 cm^{-1}, which are associated with the vibrations of the carbonyl (C=O) stretching in the imide groups. Besides, as shown in Fig. S10c**,** due to the flexibility of the C-C single bond of ethylenediamine, crystallinity of **EA-PDI** is very poor.

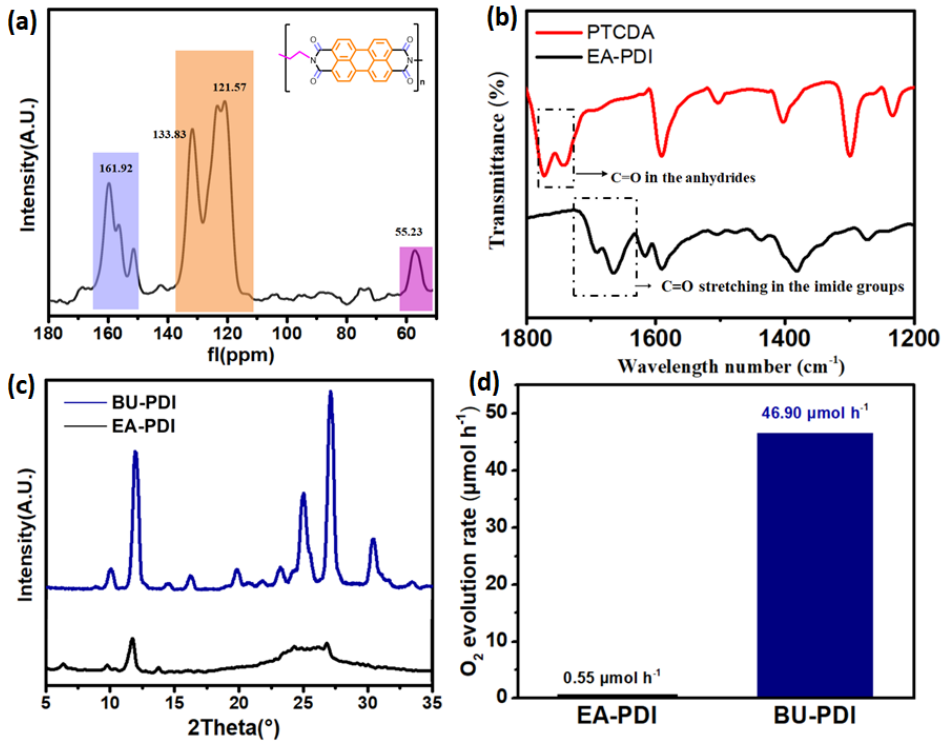

Fig. S12 Solid-state ^{13}C NMR of **EA-PDI** (a), FTIR spectra (b) Comparison of XRD patterns (c) and oxygen production performance (d) between **EA-PDI** and **BU-PDI**.

8. Recycle tests for degradation of tetracycline

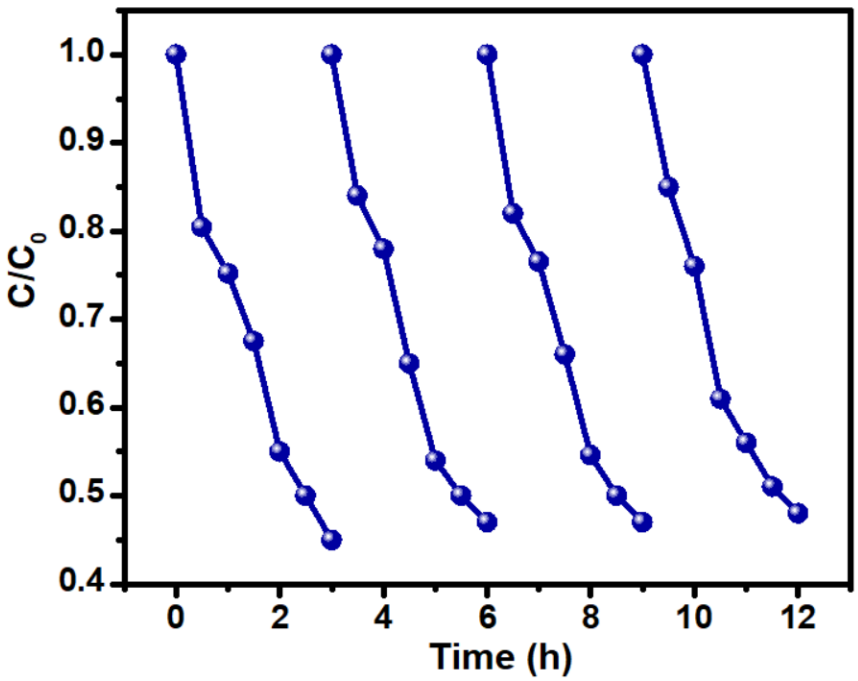

Fig. S13 Recyclability test of **BU-PDI.**

9. Electron spin resonance (ESR) spectra

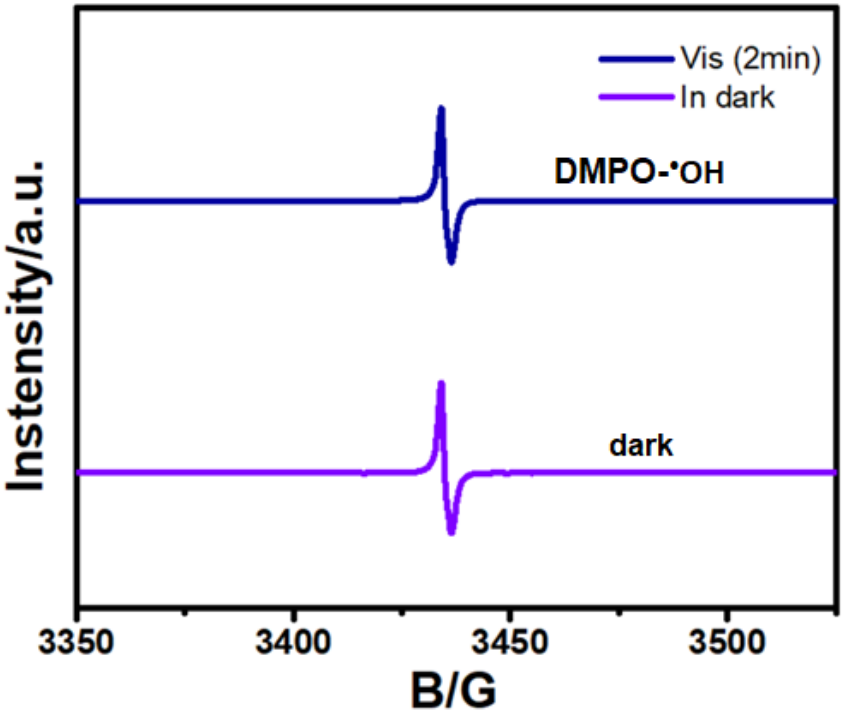

Fig. S14 ESR spectra of **BU-PDI.**

10. Details of calculation of built-in electric field magnitude

According to the literature, the built-in electric field magnitude can be measured according to the formula reported by Kanata et al.[7, 8]

$$Fs = (-2V_s\rho/\varepsilon\varepsilon_0)^{1/2}$$

Where Fs is the internal electric field magnitude, V_s is the surface potential, ρ is the surface charge density, Ɛ is the low-frequency dielectric constant, and $Ɛ_0$ is the vacuum dielectric constant. The above equation suggests that the in electric field magnitude is mainly determined by the surface voltage and the surface charge density since Ɛ and $Ɛ_0$ are two constants.

Surface voltage can be characterized by open circuit potential,[2] surface photovoltage intensity[9] and Atomic Force Microscope with a Kelvin Probe model.[2] Surface charge density can be measured by Zeta potential[10] and integrating the measured transient photocurrent density minus the steady-state values of photocurrent with respect to time.[11]

In this paper, the value of the surface voltage is determined by open circuit potential and surface charge density is calculated by integrating the measured transient photocurrent density minus the steady-state values of photocurrent with respect to time. If we normalize the value of IEF of MA-PDI as 1.0, then the relative values for U-PDI, OA-PDI and BU-PDI are 1.30, 1.40 and 1.81, respectively.

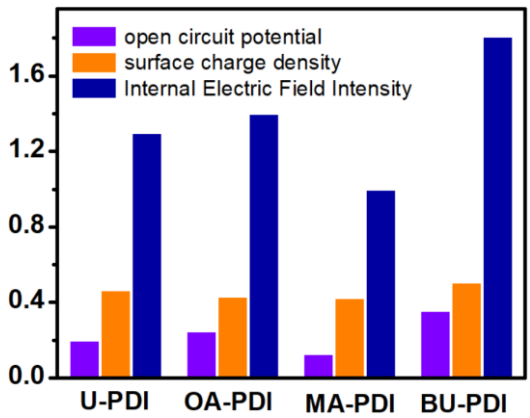

Fig. S15 Characterization of built-in electric field of **U-PDI**, **OA-PDI**, **MA-PDI** and **BU-PDI.**

11. Possible degradation pathway for tetracycline transformation

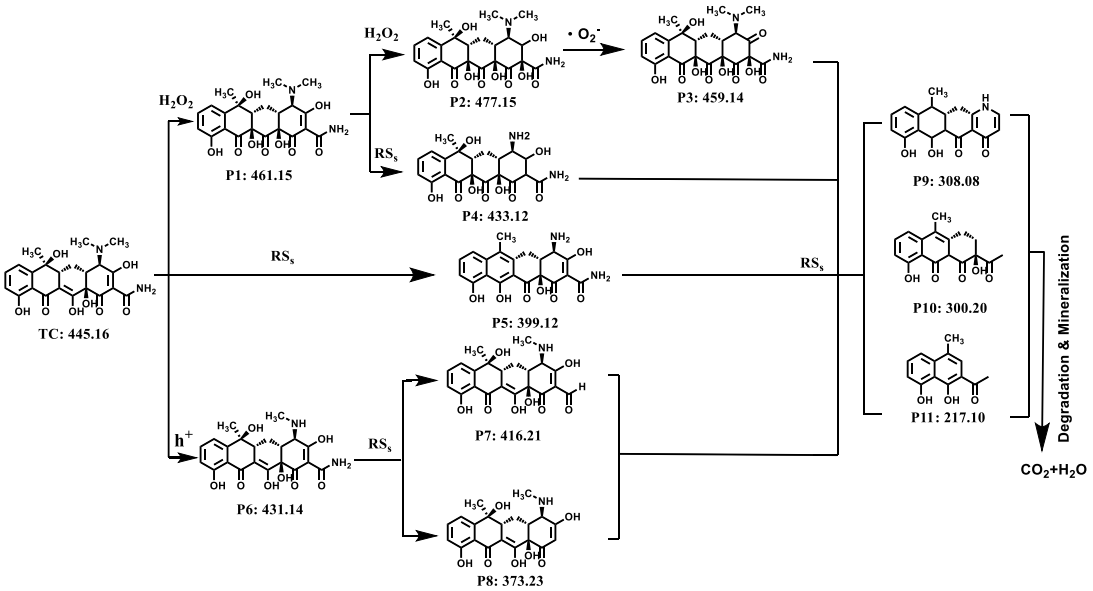

Fig. S16. Proposed degradation pathway for tetracycline transformation.

Table S4. Potential intermediates in the TC photocatalytic

TPs	Retention time (min)	m/z	Potential structure
Tetracycline (TC)	4.63	445.16	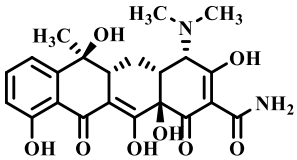
P1	4.45	461.15	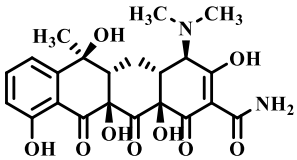
P2	5.72	477.15	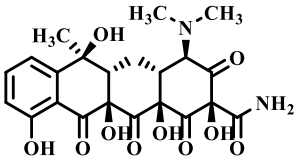
P3	4.52	459.14	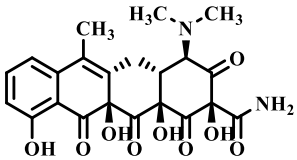

P4	4.82	433.12	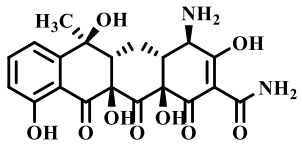
P5	6.49	399.12	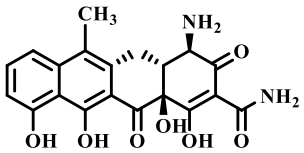
P6	3.58	431.14	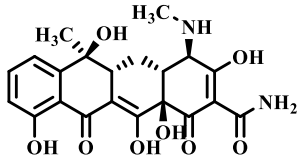
P7	7.59	416.21	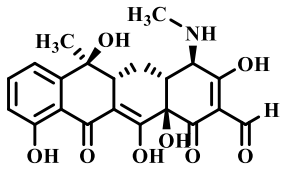
P8	5.05	373.23	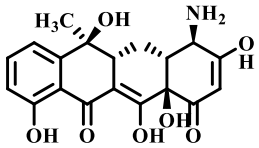
P9	5.14	308.09	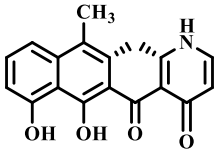
P10	4.37	300.20	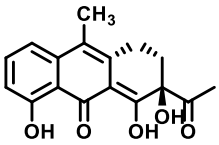
P11	4.57	217.10	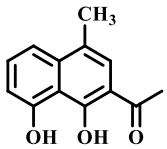

12. References

1. P. Sharma, D. Damien, K. Nagarajan, M. M. Shaijumon and M. Hariharan, *J. Phys. Chem. Lett*, 2013, **4**, 3192–3197.
2. J. Li, L. Cai, J. Shang, Y. Yu and L. Zhang, *Adv. Mater.*, 2016, **28**, 4059–4064.
3. M. Krzeszewski, E. M. Espinoza, C. Červinka, J. B. Derr, J. A. Clark, D. Borchardt, G. J. O. Beran, D. T. Gryko and V. I. Vullev, *Angew. Chem. Int. Ed.*, 2018, **57**, 12365–12369.
4. M. R. Morris, S. R. Pendlebury, J. Hong, S. Dunn and J. R. Durrant, *Adv. Mater.*, 2016, **28**, 7123–7128.
5. J. Jiang, K. Zhao, X. Xiao and L. Zhang, *J. Am. Chem. Soc.*, 2012, **134**, 4473–4476.
6. Z. Zhang, L. Wang, W. Liu, Z. Yan, Y. Zhu, S. Zhou and S. Guan, *Natl Sci. Rev*, 2021, **8**. nwaa 155.
7. K.-K. Takashi, M. Masayuki, T. Hideyuki, H. Yoshihiro and N. Taneo, in *Proc. SPIE*, 1990.
8. Z. Zhang, X. Chen, H. Zhang, W. Liu, W. Zhu and Y. Zhu, *Adv. Mater.*, 2020, **32**, e1907746.
9. X. Chen, J. Wang, Y. Chai, Z. Zhang and Y. Zhu, *Adv. Mater.*, 2021, **33**, e2007479.
10. J. Li, G. Zhan, Y. Yu and L. Zhang, *Nat. Commun*, 2016, **7**, 11480.
11. F. Le Formal, K. Sivula and M. Grätzel, *J. Phys. Chem. C*, 2012, **116**, 26707–26720.